Radiometric Cross-Calibration of GF-4/VNIR Sensor With Landsat8/OLI, Sentinel-2/MSI, and Terra/MODIS for Monitoring Its Degradation

Caixia Gao [ID], Yaokai Liu [ID], Shi Qiu, Chuanrong Li [ID], Lingling Ma [ID], Qijin Han, Jingru Liu, Enyu Zhao, Yongguang Zhao [ID], Yonggang Qian [ID], and Ning Wang [ID]

Abstract—Optical satellite sensor generally suffers from drifts and biases relative to their prelaunch calibration, caused by launch and the space environment. Radiometric cross-calibration is valuable for calibrating sensors without coincident surface measurements through transferring radiometric values between satellite sensors via a stable target. The data quality of visible and near-infrared (VNIR) sensor onboard Gaofen-4 (GF-4) satellite seriously depends on vicarious calibration, which is performed once every year, thus, a cross-calibration approach is proposed for monitoring its radiometric performance much more frequently. In this study, the GF-4/VNIR is cross-calibrated by Landsat8/OLI, Sentinel-2/MSI, and Terra/MODIS with the aid of the tandem scenes during 2017 and 2018 after correcting the discrepancy on viewing geometries and spectrum. The results show that there is test site dependency and sensor dependency, and cross-calibration coefficients in the four bands roughly have similar variation trend as a sinusoidal function during 2017 and 2018, varying from 0.00023 to 0.00079. Furthermore, uncertainty analysis of the cross-calibration is carried out to analyze the uncertainty contributions affecting the cross-calibration accuracy. Note that the calibration accuracy of referenced sensors, the uncertainty of the MODTRAN model, BRDF uncertainty are the three main factors affecting the cross-calibration accuracy, the total uncertainty is approximately 3.9%–6.64%.

Index Terms—Bidirectional reflectance distribution function model, cross-calibration, Gaofen-4/visible-light and near-infrared (GF-4/VNIR), Landsat8/OLI, Spectral adjustment, Sentinel-2/MSI, Terra/MODIS.

Caixia Gao, Yaokai Liu, Shi Qiu, Chuanrong Li, Lingling Ma, Jingru Liu, Yongguang Zhao, Yonggang Qian, and Ning Wang are with the Key Laboratory of Quantitative Remote Sensing Information Technology and Aerospace Information Research Institute, Chinese Academy of Sciences, Beijing 100094, China (e-mail: gaocaixia@aoe.ac.cn; liuyk@aoe.ac.cn; sqiu@aoe.ac.cn; crli@aoe.ac.cn; llma@aoe.ac.cn; jingruliu_1@163.com; ygzhao@aoe.ac.cn; qianyg@aoe.ac.cn; wangning@aoe.ac.cn).

Qijin Han is with the China Centre for Resources Satellite Data and Application, Beijing 100094, China (e-mail: cresda_hanjin@126.com).

Enyu Zhao is with the College of Information Science and Technology, Dalian Maritime University, Dalian 116026, China. (e-mail: zhaoenyu@dlmu.edu.cn).

Digital Object Identifier 10.1109/JSTARS.2020.2991214

I. INTRODUCTION

CONSIDERABLE effort went into the design and development of earth observation (EO) sensors, resulting in many stable sensors ever, such as Landsat/TM, Landsat7/ETM, Terra/MODIS, NPP/VIIRS, etc. For quantitative applications to make full use of the ever-increasing number of EO satellite systems, data from the various imaging sensors involved must be on a consistent radiometric scale [1]–[3]. A sound calibration of the individual sensors is critical for ensuring their data quality, and assessing consistency between different sensors.

Right now, several approaches to postlaunch radiometric calibration have been well documented, which are based on reference to onboard standards, solar and lunar illumination, and ground-based test sites [4], [5]. Earth surface with suitable characteristics has long been used to transfer radiometric standards between satellite sensors, such as vicarious calibration and cross-calibration [1], [6]. The vicarious calibration relies on ground truth measurements coincident with a sensor overpass for driving radiative transfer code MODTRAN to generate the radiance at the top of atmosphere (TOA), and then TOA radiance values are compared against the sensor digital numbers (DNs) to determine the radiometric calibration coefficients. This method requires high accuracy for coincident measurements of surface and atmospheric characteristics, and the overall uncertainty seriously depends on the accuracy of measurements. In addition, the cross-calibration technique is meant for calibrating sensors through comparisons of band-to-band data of which spectral response functions (SRFs) are overlapped mostly [7]. This method does not require simultaneous measurements, and ideally, the derived results when viewing the same source at the same time, will agree within the stated uncertainties of the sensors. Such a method is effectively one for assessing consistency between different sensors, and the National Environmental Satellite, Data, and Information Service has been developed the simultaneous Nadir overpass (SNO) method for intersatellite calibration in the last few years with excellent results [8], [9]. However, it relies on near-simultaneous observations from sensors in polar regions only, and this limits the approach since it requires both sensors are coincident in time with identical view and solar geometries, which happen randomly, especially for high-resolution sensor onboard polar orbit. In consideration of this, the extended SNO (SNOx) provides an opportunity to compare satellite instruments

at low latitudes over wide dynamic ranges [10], such as over ocean surface, desert targets, green vegetation, etc. Its calibration uncertainty is mainly caused by the spectral, temporal and viewing angle differences, and colocation error among different sensors. To reduce these uncertainties in the cross-calibration processing, various schemes are investigated. Teillet *et al*. developed a technique to account for small changes in view and solar geometry by deriving the surface reflectance of a test site both spatially and spectrally [11], and this approach allowed the intercomparison of a wide array of sensors viewing a test site on a single day but at varying times and with varying view angles. In consideration of the surface bidirectional reflectance distribution function (BRDF), Liu *et al*. [12] and Gao *et al*. [6] developed a new method for cross-calibration, and then applied the method to MVIRS, VIRR onboard Fengyun (FY) satellite and MODIS instrument onboard Terra satellite. Teillet *et al*. [4] also investigated impact of spectral response difference effect between sensors as quantitative indication using simulated data of observation.

Gaofen-4 (GF-4) is the first geosynchronous orbit remote sensing satellite in the significant special space-based system of the national high-resolution earth observation system. It was launched on December 29, 2015, and equipped with one stare camera with a resolution of 50 m in visible and near-infrared spectrum, and of 400 m in medium infrared spectrum. As the highest spatial resolution among the civil satellite on the geosynchronous orbit, GF-4 satellite has 4 operation mode: general, continuous, regional, and maneuvering, and has great potential for environmental protection, marine, agriculture, and water conservation as well as regional application [13]. The GF-4 satellite is not equipped with an onboard calibrator, the in-orbit radiometric calibration seriously depends on the vicarious calibration in Dunhuang test site. And this vicarious is performed once per year due to the high cost of manpower, material, and financial resources. Therefore, cross-calibration is an excellent method for monitoring its radiometric performance and assessing consistency with other sensors using Landsat8/OLI, and Sentinel-2/MSI, and Terra/MODIS, which are equipped with stable and high-accuracy onboard calibrators to ensure its data quality. In this cross-calibration, a method associated with temporal, viewing angle, and spectral correction is used to improve calibration accuracy.

In this study, the test site and datasets are described in Section II. Section III gives the cross-calibration method. The long-term cross-calibration result of GF-4/visible and near-infrared (VNIR) against Landsat8/OLI, and Sentinel-2/MSI, and Terra/MODIS is presented in Section IV. The uncertainty analysis of the cross-calibration is shown in Section V. The conclusion is drawn in Section VI.

II. DESCRIPTIONS OF TEST SITE AND DATASETS

In order to collect much more calibration samples for monitoring the degradation of GF-4/VNIR sensor, the Dunhuang site, Dalate site, and Baotou site in China have been used as stable ground target for transferring the radiometric values. In this section, the characteristics of the three test sites, and the corresponding datasets used are depicted as follows.
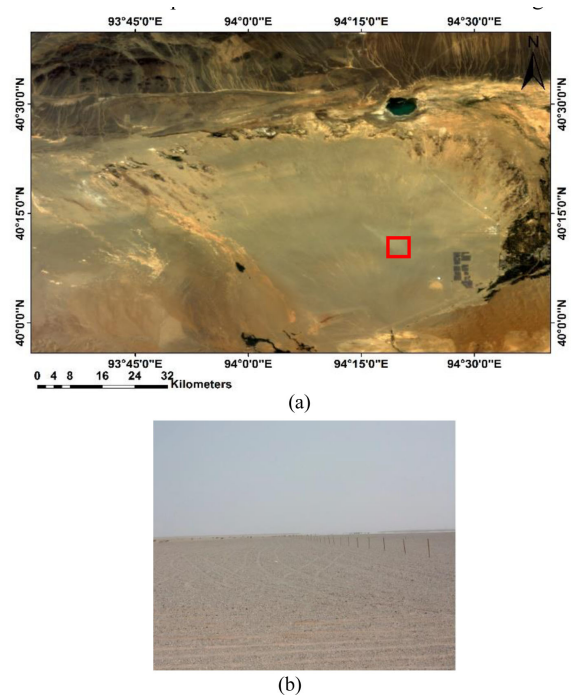

(a)

(b)

Fig. 1. Dunhuang site: (a) GF-4/VNIR image on September 5, 2017, and (b) detailed landscape of the calibration area represented by the red box in VNIR image.

A. Test Sites

Dunhuang, Dalate, and Baotou test sites are excellent spatial uniformity and temporal stability. Despite these sites are not perfectly Lambertian, the direction variation of their reflectance was monitored using different sensors or ground-based instruments. Therefore, these sites in China are selected to carry out the cross-calibration, and their characteristics are described in detail as following.

1) Dunhuang Site: Dunhuang test site is located in 20 km northwest of Dunhuang in Gansu province, with geographic coordinates of 40.04 °N–40.28 °N and 94.17 °E–94.5 °E. The overall size of the playa is approximately 20 × 30 km with an elevation of approximately 1.19 km. The site is spatially uniform with a coefficient of variation (standard deviation/mean) less than 2% of spectral reflectance over the 10 × 10 km central region. Its surface reflectance is about 15%–30% from the visible to near-infrared (NIR) spectral region, and it characterizes low aerosol loading except for the dusty spring season from March to May. The Dunhuang test site was selected in 2008 by the Working Group on Calibration and Validation (WGCV) of the Committee on Earth Observation Satellites (CEOS) as one of the instrumented references sites, and has been used as an excellent earth target for vicarious calibration and cross-calibration for optical sensors. The GF-4/VNIR image on September 5, 2017, over Dunhuang site and the detailed landscape of the calibration area are shown in Fig. 1.

2) Dalate Site: Dalate test site is located at the Southwest of Kubuqi desert, which is the seventh biggest desert in China covering an area of about $18\,600\,km^2$. It has a plateau continental
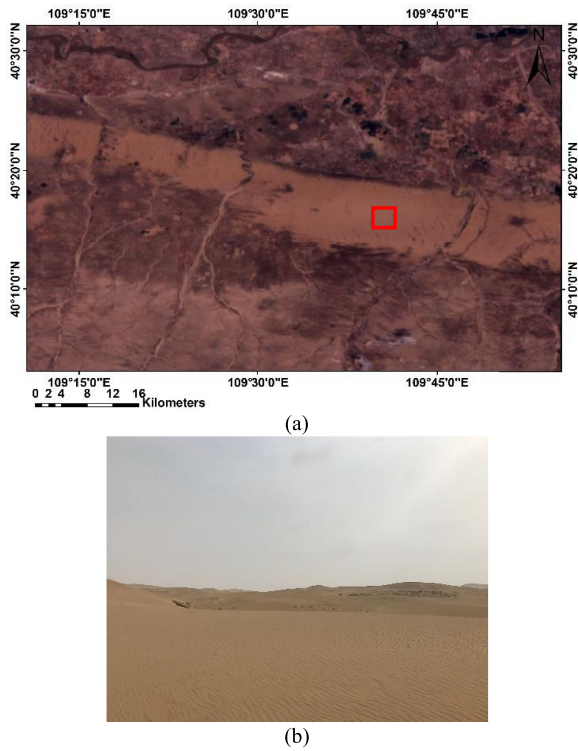
Fig. 2. Dalate site: (a) GF-4/VNIR image on September 28, 2017, and (b) detailed landscape of the calibration area represented by the red box in VNIR image.
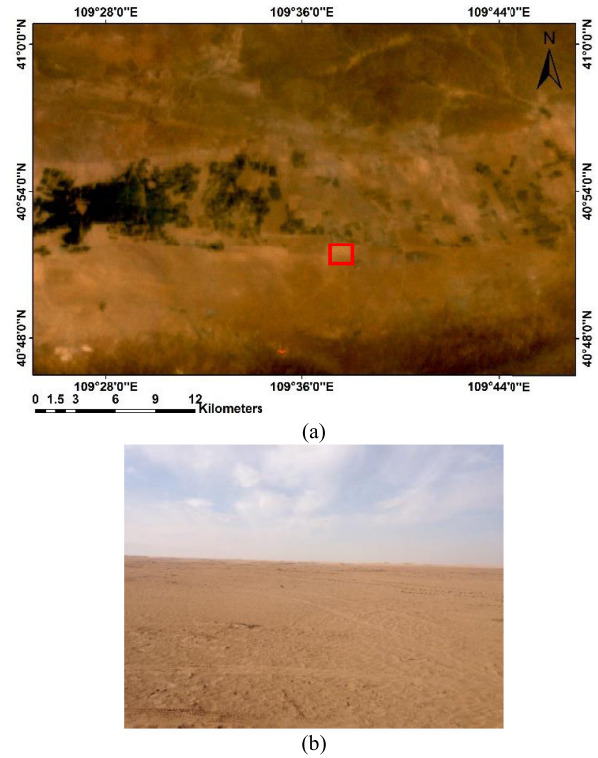

Fig. 3. Baotou site: (a) GF-4/VNIR image on July 1, 2017, and (b) detailed landscape of the calibration area represented by the red box in VNIR image.

climate with a cold semi-arid climate. The average annual rainfall is about 400 mm in Kubuqi desert, China. The calibration test site has a geographical area of 40.23 °N–40.25 °N, 109.85 °E–109.88 °E. Comparing with Baotou sandy site, Dalate test site has much bigger size, and has a spatial uniform with a coefficient of variation (standard deviation/mean) less than 2% derived from GF-4/VNIR image. It is suitable for the cross-calibration of the moderate resolution sensors, such as MODIS, AVHRR, etc. The GF-4/VNIR image on September 28, 2017 over Dalate site and the detailed landscape of the calibration area are shown in Fig. 2.

3) Baotou Site: Baotou site is located in the Inner Mongolia, China, 50 km away from Baotou city with convenient transportation. It covers a flat area of approximately 300 km^2 with an average altitude of 1270 m, and features a cold semi-arid climate. The site is dominated by various land surfaces, including lake, sand, bare soil, maize, grass, etc., and is equipped with various artificial standard targets and natural scenes, including portable and permanent targets. As part of the contribution to worldwide calibration and validation study coordinated by CEOS-WGCV, Baotou site is offering its support to Radiometric Calibration Network of Automated Instruments (RadCalNet), with an aim of providing demonstrated global standard automated radiometric calibration service in cooperation with the European Space Agency, the National Aeronautics and Space Administration, the National Centre for Space Studies (CNES) and the National Physical Laboratory. The sandy area in this site has an area of 300 × 300 m with a uniformity of approximately 2% [14], which is used as a stable ground target for this cross-calibration. The

GF-4/VNIR image on July 1, 2017, over Baotou site and the detailed landscape of the calibration area is shown in Fig. 3.

B. Datasets

We choose 2017 and 2018 as the study year for all the datasets in this research. To avoid the impact of clouds on the satellite observation, total 32 clear-sky datasets during 2017 and 2018 are used in the analysis. For clarity, the satellite images, BRDF data, and the corresponding atmosphere parameters are described as follows.

1) Satellite Image Datasets: GF-4/VNIR provides images in 5 spectral bands ranging in wavelengths from 0.45 to 0.90 μm, with a spatial resolution of 50 m at nadir. It seriously depends on vicarious calibration to ensure its data quality. In this study, GF-4/VNIR band 2–5, namely blue band, green band, red band, NIR band, is cross-calibrated with the corresponding bands from Landsat8/OLI (band 2, band 3, band 4, and band 5), Sentinel-2/MSI (band 2, band 3, band 4, and band 8) and Terra/MODIS (band 3, band 4, band 1, and band 2), respectively. Landsat8/OLI observes a 185 km wide swath of the Earth in 30 m resolution at nadir; Sentinel-2/MSI measures the Earth's reflected radiance at 30-m resolution at nadir; whereas, MODIS captures data in band 1, 2 at 250-m spatial resolution and band 3, 4 at 500-m spatial resolution. To reduce the spatial discrepancy between two sensors, the reference and the to-be-calibrated data should be geometrically registered.

The sensor characteristics of GF-4/VNIR, Landsat8/OLI, Sentinel-2/MSI, and Terra/MODIS in these selected bands are

TABLE I
SENSOR CHARACTERISTICS OF GF-4/VNIR, LANDSAT8/OLI, SENTINEL-2/MSI,
TERRA/MODIS IN SELECTED BANDS

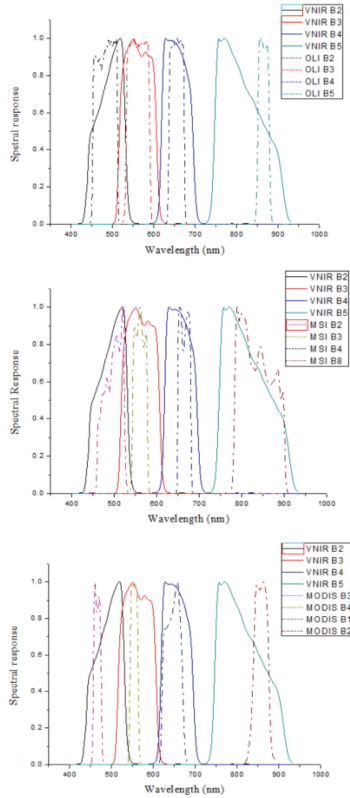| Sensor	Band number	Centre wavelength(nm)	Spectral range (nm)	Spatial resolution(m)
VNIR	2	519	450–520	
	3	550	520–600	
	4	628	630–690	50
	5	770	760–900	
OLI	2	482.6	450–510	
	3	561.3	530–590	
	4	654.6	630–670	30
	5	864.6	850–880	
MSI	2	492.4	458–523	
	3	559.8	543–578	
	4	664.6	650–680	10
	8	832.8	785–900	
MODIS	3	470	459–479	500
	4	555	545–565	
	1	645	620–670	250
	2	865	841–876	

Fig. 4. SRFs for these selected bands of GF-4/VNIR, Sentinel-2/MSI, and Terra/MODIS.

shown in Table I, and the corresponding SRFs are shown in Fig. 4.

Since the two sensors onboard different platforms have different overpassing times, the difference in data acquisition time of the tandem scene is required within 1 h for balancing amount of the calibration samples and the atmospheric effect. The viewing geometries of the 32 clear-sky tandem scenes over the Dunhuang
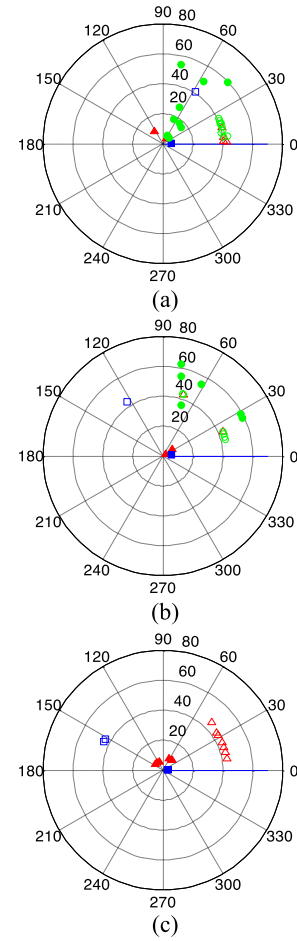

Fig. 5. Viewing geometries of referenced sensor and recalibrated sensor. (Solid symbol represents reference, hollow symbol represents to-be-calibrated; the red one represents the data pair of MSI and VNIR, the blue one represents the data pair of OLI and VNIR, the green one represents the data pair of MODIS and VNIR). (a) Dunhuang site. (b) Dalate site. (c) Baotou site.

site, Dalate site, and Baotou site during 2017 and 2018 are shown in Fig. 5. Note that some of the data pairs have large differences in viewing direction between the two sensors, and a model should be proposed to correct the radiance difference resulting from the viewing geometries.

2) BRDF Datasets: BRDF is an inherent optical property that describes the reflectance of a surface when illuminated by an infinitesimally narrow beam of radiation, and viewed through an equally infinitesimally narrow beam, and is a function of the geometry of those two beams [15]. It is a theoretical parameter impossible to measure directly, therefore, the bidirectional reflectance factor (BRF) is still defined with infinitesimal reflected solid angles which make it as conceptual as BRDF. In this study, the *in situ* measurements of BRF characteristics over Dunhuang and Baotou sites are collected using SVC HR1024 spectrometer and multiangle observation system under clear-sky condition and solar zenith angle (SZA) of 30˚. The spectrometer is designed to scan at the relative azimuth angles (RAA) from 0˚ to 360˚ with a step of 30˚, viewing zenith angle (VZA) from 0˚ to 30°with a step of 5˚ for Baotou site, and from 0˚ to 70˚ with a

step of 14° for Dunhuang site. The BRF measurements, whose VZAs are within 30°, are selected to fit the Ross-Li BRDF model [16], [17] for constructing the surface anisotropic effects, so that the BRFs (R) can be corrected to a nadir view geometry.

The Ross-Li BRDF model decomposes surface reflectance into three types of scattering, and combines them in the following form:

$$R(\theta_i, \theta_v, \varphi, \lambda) = f_{\text{iso}}(\lambda) + f_{\text{vol}}(\lambda)K_{\text{vol}}(\theta_i, \theta_v, \varphi, \lambda)$$
$$+ f_{\text{geo}}(\lambda)K_{\text{geo}}(\theta_i, \theta_v, \varphi, \lambda) \qquad (1)$$

where θ_i is SZA, θ_v is VZA, φ is RAA, λ is wavelength, K_{vol} and K_{geo} are the volumetric and geometric scattering kernels, respectively, and f_{iso}, f_{vol}, and f_{geo} are the isotropic, volumetric, and geometric kernel scaling parameter, respectively. In practice, a linear least square fitting is used to find the best kernel scaling parameters.

In addition, since the *in situ* BRF measurements are not available for Dalate site, MODIS BRF product (MCD 43A1) are used to minimize the viewing and illumination effects on the cross-calibration. It provides the model parameters of Ross-Li BRDF model at overlapping 8-day "weekly" intervals based on 7 spectral bands, and model parameters for corresponding data pairs are extracted from MCD 43A1 product for BRF estimation.

Fig. 6(a)–(c) shows the multiangle BRF simulated in NIR band over the three test sites, respectively. The uncertainty of the fitted Ross-Li BRDF model is approximately 5%, and it is noted that the general increasing trend towards the backward scattering direction is presented in Fig. 6.

3) Water Vapor Data: The MODIS precipitable water product (MOD 05) consists of column water vapor (WVC) amounts. During the daytime, a NIR algorithm is applied over clear land areas of the global and above clouds over both land and ocean; over clear ocean areas, water vapor estimates are provided over the extend glint area [18]. The WVC retrieved from NIR radiation received by the sensor and the corresponding quality assurance scientific data sets (SDSs) are stored at a spatial resolution of 1 km. In addition, the SDSs related to time, geolocation, and viewing geometry are only stored at 5-km pixel resolution. In this study, according to the SDSs information, WVC for each tandem scene is mainly extracted from water vapor product at a spatial resolution of 1 km in MOD 05 product since the WVC variation could be neglected within 1 h. However, due to its data missing for these tandem scenes on October 31, 2017, May 29, 2018, June 14, 2018, and December 8, 2017, the WVC extracted from National Centers for Environmental Prediction reanalysis dataset is numerically interpolated to acquire the values at the scenes' acquisition time [19], which provides meteorological parameters at a spatial resolution of 2.5 degree every 6-hourly observations. Fig. 7 shows WVC for each tandem scene. It is noted that the maximum WVC is lower than 3 g/cm^2.

4) Aerosol Data: The VIIRS aerosol data products are derived primarily from the radiometric channels covering the visible through the short-wave infrared spectral regions (412–2250 nm). The Intermediate Product (IP) of VIIRS is aerosol retrieval at the pixel level with a high spatial resolution of 750 m [20]. It consists of aerosol optical depth (AOD) at 550 nm,
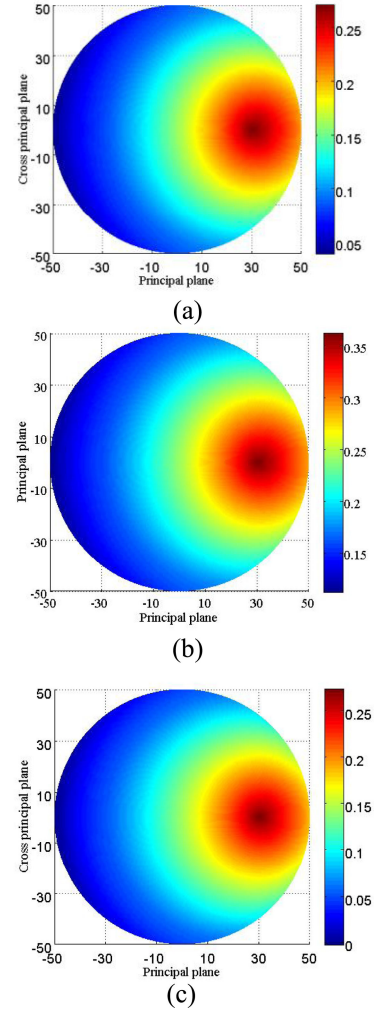

(a)

(b)

(c)

Fig. 6. Polar plot of BRF simulation data in NIR band over the three test sites for SZA = 30°. Polar angles represent RAA with a zero degree pointing to the East, and the circle radius direction represents the variation of VZA from 0° to 50°. (a) Dunhuang site. (b) Dalate site. (c) Baotou site.

Ångström exponent, and aerosol model information including a single-aerosol model selected over land and three parameters retrieved over the ocean. IP is averaged and aggregated to an Environmental Data Record (EDR) with a spatial resolution of 6 km (8 × 8 pixels). AOD data is extracted from the VIIRS EDR data for avoiding the data missing in several study dates, and is directly used in this cross-calibration since the temporal variation of AOD under a clear sky is relatively small during a time span of 3 h, which is the maximum differences on image acquisition time between VNIR and VIIRS. Fig. 8 also shows the AOD data for each tandem scene. Note that the maximum AOD is lower than 0.45.

III. CROSS-CALIBRATION METHOD

In order to eliminate the spectral and angular discrepancies between two sensors, a cross-calibration approach based on a radiative transfer model is used in this study.
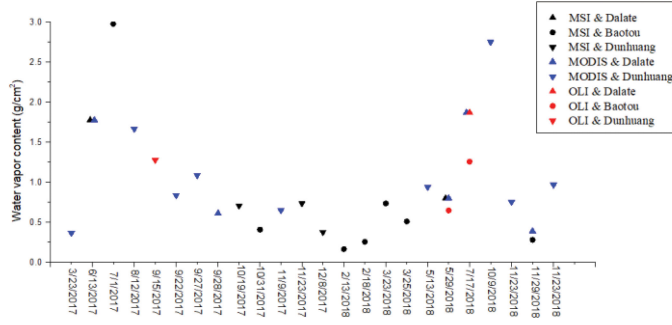
Fig. 7. Water vapor content at the data acquisition time of Sentinel-2/MSI, Landsat8/OLI, and Terra/MODIS over Dunhuang, Dalate, and Baotou sites.
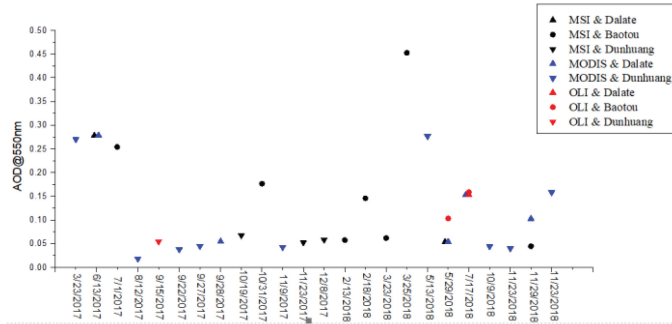

Fig. 8. Aerosol optical depth @ 550 nm at the data acquisition time of Sentinel-2/MSI, Landsat8/OLI, and Terra/MODIS over Dunhuang, Dalate, and Baotou sites.

A. Cross-Calibration Formulation

The radiance received by a sensor in spectral band i L_i can be described by the following equation:

$$Q_i = G_i L_i + Q_{0i} \qquad (2)$$

where Q_i is digital counts in spectral band i, G_i is band-averaged sensor responsivity (in counts per unit radiance), and Q_{0i} is the zero-radiance bias (in counts).

TOA reflectance ρ_i^* is related to the TOA radiance by

$$\rho_i^* = \pi L_i d_s^2 / (E_{0i} \cos \theta) \qquad (3)$$

where d_s is the Earth–Sun distance in astronomical units, E_{0i} is the exo-atmospheric solar irradiance in spectral band i, and θ is the solar zenith angle. A combination of (2) and (3) yields

$$\Delta Q_i = Q_i - Q_{i0} = \rho_i^* G_i E_{0i} \cos\theta / \pi d_s^2. \qquad (4)$$

Thus, the cross-calibration formulation between GF-4/VNIR [denoted as GF in (5)] and the references [denoted as REF in (5)] can be described as

$$\Delta Q_{i(\text{GF})} = (G_{i(\text{GF})}/G_{i(\text{REF})}) \times (\rho_{i(\text{GF})}^*/\rho_{i(\text{REF})}^*)$$

$$\times (E_{0i(\text{GF})}/E_{0i(\text{REF})}) \times (\cos\theta_{\text{GF}}/\cos\theta_{\text{REF}}) \times \Delta Q_{i(\text{REF})}$$

$$K = (\rho_{i(\text{GF})}^*/\rho_{i(\text{REF})}^*) \qquad (5)$$

where K is a factor related to spectral band adjustment and viewing geometry correction between GF-4/VNIR and the references.
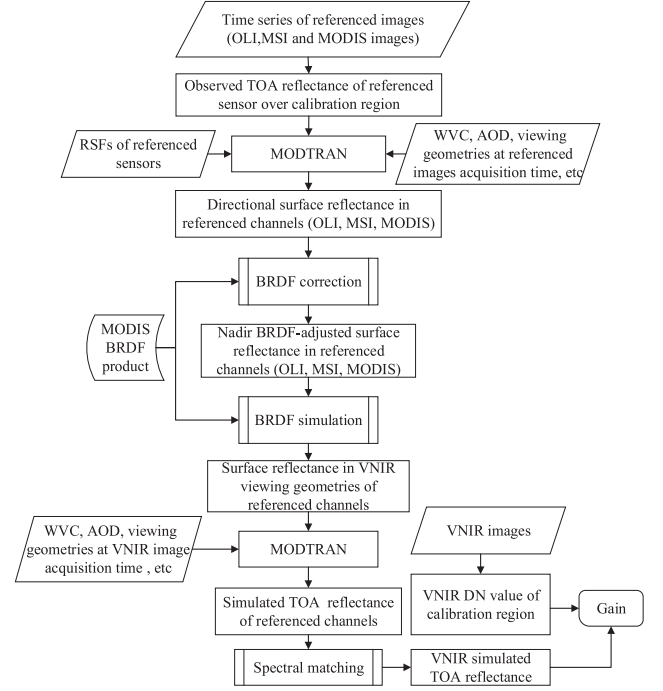

Fig. 9. Flowchart of the cross-calibration method.

B. Angular Difference Correction

Since each instrument can measure radiance from the collocation targets in different viewing geometry, it is possible to account for the angular differences by considering a radiative transfer model MODTRAN and Ross-Li BRDF model. First, the directional reflectance at the bottom of atmosphere (BOA) over test site is derived from the TOA reflectance of referenced sensor $\rho_{i(\text{REF})}^*$ using the MODTRAN model with necessary inputs, such as the viewing geometry of the referenced sensor, WVC, AOD, etc. And then, it is corrected to the nadir BRDF-adjusted surface reflectance in referenced channels with the aid of Ross-Li BRDF model. Subsequently, the directional surface reflectance of referenced channels in GF-4/VNIR viewing geometry is derived by BRDF model, and the corresponding TOA reflectance can be simulated using MODTRAN model driving by the viewing geometry of the GF-4/VNIR, WVC, aerosol data, etc. (see Fig. 9).

C. Spectral Matching

There are significant differences in relative spectral response profiles between two sensors, even for spectral bands designed to look at the same region of the electromagnetic spectrum. It is essential to compensate for the spectral band differences of multispectral sensors to provide a more accurate cross-calibration between the sensors. The effect of spectral band difference on measured TOA reflectance depends on spectral variation in the exo-atmospheric solar illumination, the atmospheric transmittance, and the surface reflectance. Therefore, in this study, spectral adjustment coefficient for tandem scenes is acquired with the simulated TOA reflectance in corresponding band of

GF-4/VNIR and the referenced band. The surface reflectances, varying from 0.1 to 0.5 with a step of 0.1, are used as inputs to drive the MODTRAN model, together with selected atmospheric states, sensor's SRF, and the illumination and viewing geometries. Note that we adopt the viewing geometry of GF-4/VNIR for avoiding the influence of VZA differences. The detailed viewing geometries and atmosphere parameters involved in the simulations are given in Section II-B. *K* factors for each tandem scene is calculated by linearly fitting the simulated TOA reflectance in GF-4/VNIR band and that in the referenced band.

After spectral matching, the simulated GF-4/VNIR TOA reflectance is acquired and can be compared with the DN value in GF-4/VNIR images over calibration region to calculate the gain factor in each band (see Fig. 9).

IV. RESULT

To perform this cross-calibration, common calibration areas over the three sites are selected as regions of interesting (ROIs) and are geometrically registered with each other. Meanwhile, due to the different spatial resolution of data pairs, the DN values of ROIs are averaged and are converted into units of TOA reflectance using calibration coefficients. Subsequently, with the aid of atmosphere data (see Figs. 7 and 8), the atmosphere correction is performed for the referenced sensor via MODTRAN model, Fig. 10 shows the scatter-plot of TOA reflectance against BOA reflectance of referenced sensors from ROI over Dunhuang, Dalate, and Baotou sites. Noted that the atmosphere effect in the blue band is higher than that in the other three bands due to strong scattering in the blue band. Furthermore, the differences in Fig. 11 denote the sole influence of the BRDF correction with positive or negative values, which depend on differences between the viewing geometries of the two sensors (see Fig. 5). Subsequently, with the aid of atmosphere parameters, the simulated TOA reflectance in the corresponding band of the referenced sensor at GF-4/VNIR viewing direction is generated and is spectrally corrected using the spectral adjustment factor to acquire the simulated TOA reflectance of GF-4/VNIR. Fig. 12 gives spectral band adjustment factors between GF-4/VNIR and referenced sensors over the three test sites. The simulated TOA reflectance of GF-4/VNIR is shown in Fig. 13 and is compared with the DN values in the GF-4/VNIR images over the ROIs of the three sites (see Fig. 14) for calculating the cross-calibration coefficient (gain) of GF-4/VNIR during 2017 and 2018. For reading clarity, the gain values are magnified to 1000 times their actual one in Fig. 14. Note that the gain factor is test site dependency and sensor dependency, which would be caused by the spectral correction, registration of the common areas used for the cross-calibration, and temporal variability in the sensors relative to one another. Similar conclusion also was reported in [21]. The cross-calibration coefficients in the four bands present a season fluctuation might be due to periodical change on geometrical configurations; they roughly have a sinusoidal trend variation, varying from 0.00023 to 0.00079. In addition, a linear fitting is carried out for analyzing the degradation. It is
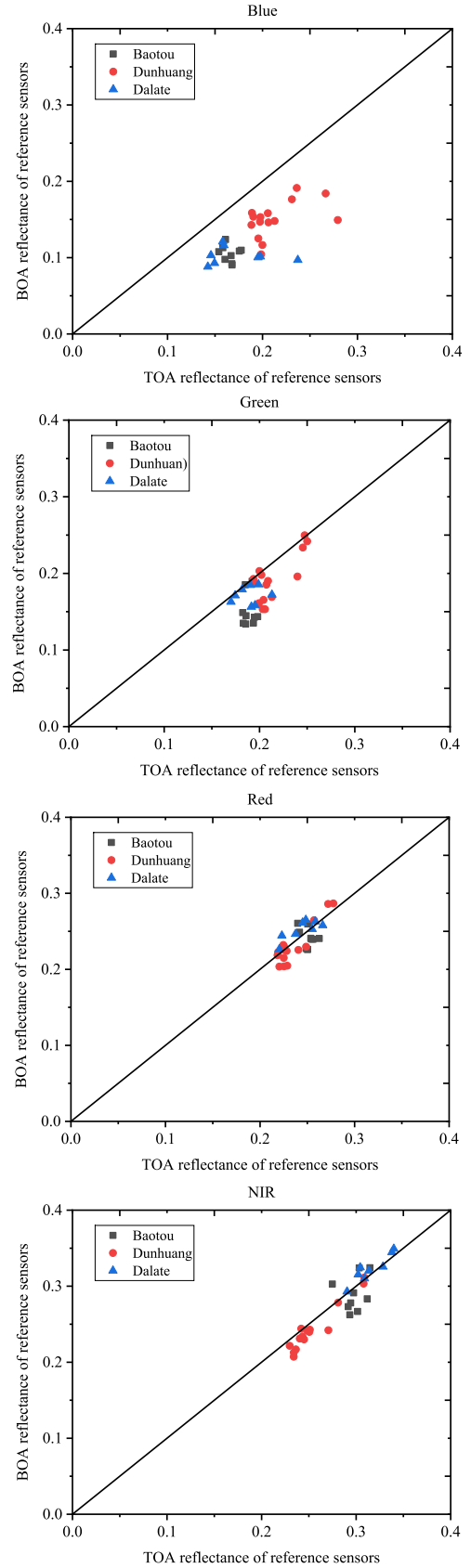

Fig. 10. Scatter plot of TOA reflectance against the derived directional BOA reflectance of referenced sensors.
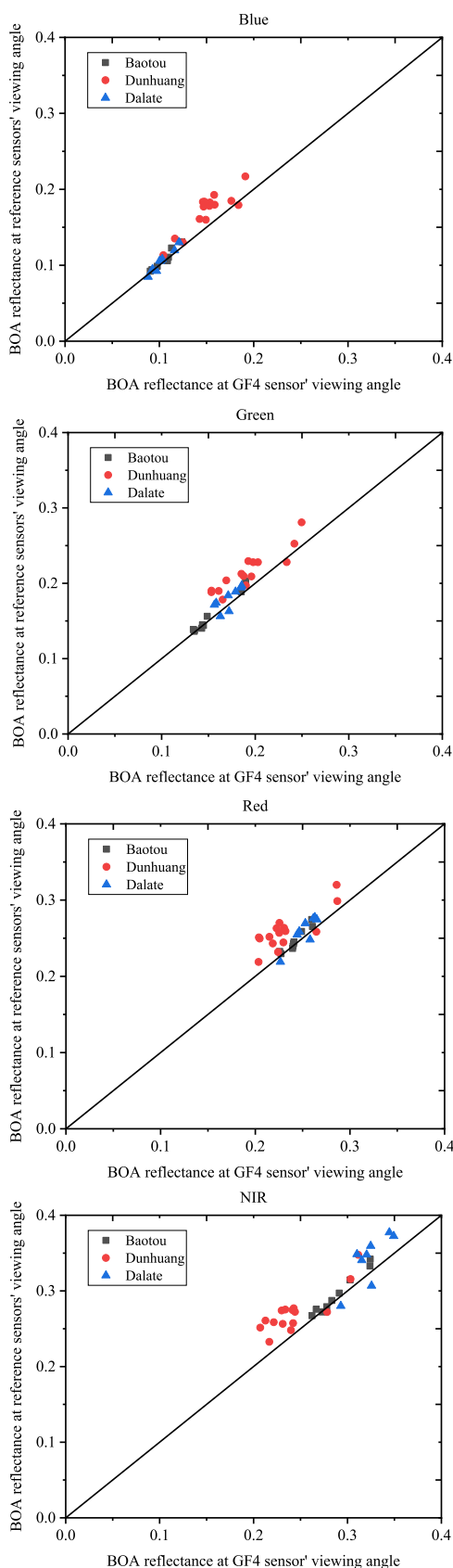
Fig. 11. Scatter plot of the derived directional BOA reflectance of referenced sensors against the directional BOA reflectance at GF-4 sensor's viewing direction.
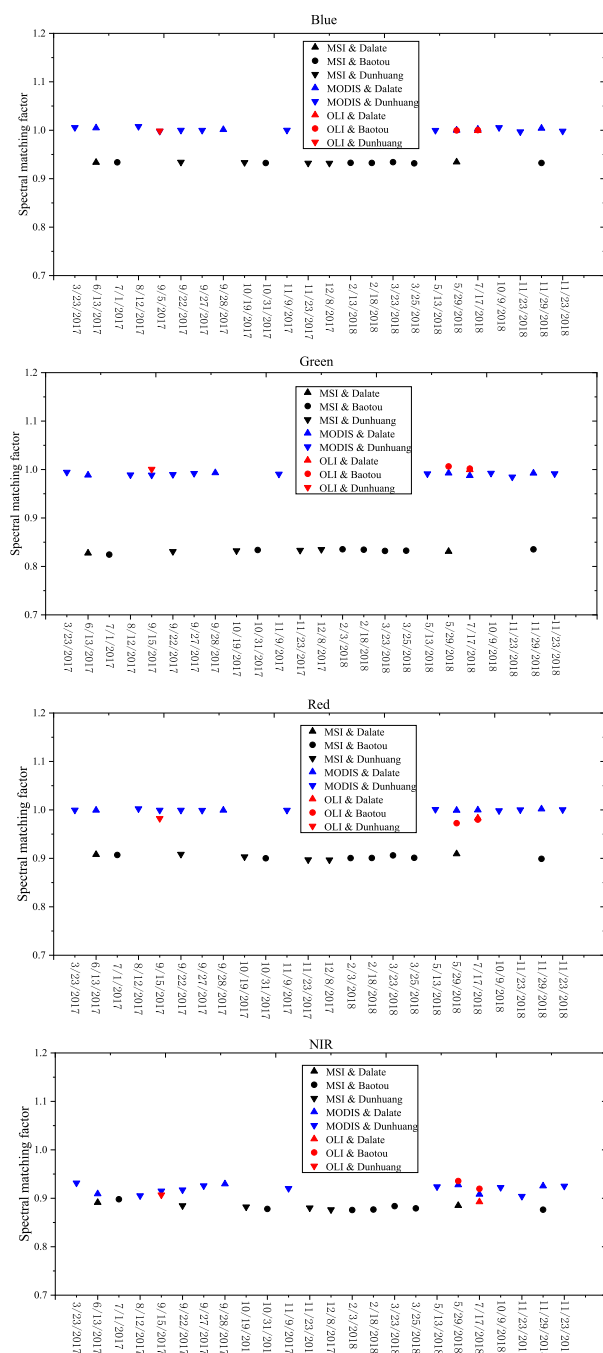
Fig. 12. Spectral band adjustment factor between GF-4/VNIR and referenced sensors.

noted from Fig. 14 that a decreasing trend is given during 2017 and 2018.

Furthermore, in order to validate the cross-calibration results, four match-ups are selected over Baotou site due to the lack of synchronous *in situ* measurements over Dunhuang and Dalate sites, namely these datasets on July 1, 2017, October 31, 2017, March 23, 2018, and November 23, 2018. With the aid of surface reflectance and synchronous atmosphere parameters (WVC, AOD), the TOA reflectance of GF-4/VNIR is simulated using
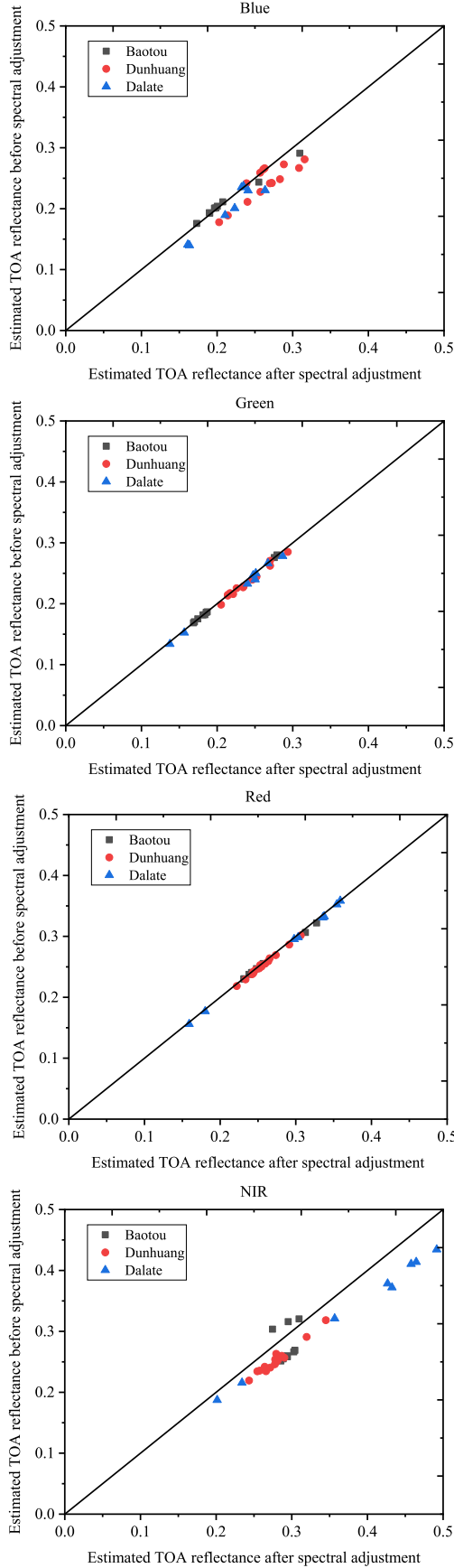
Fig. 13. Scatter plot of simulated TOA reflectance of GF-4 after and before spectral adjustment.
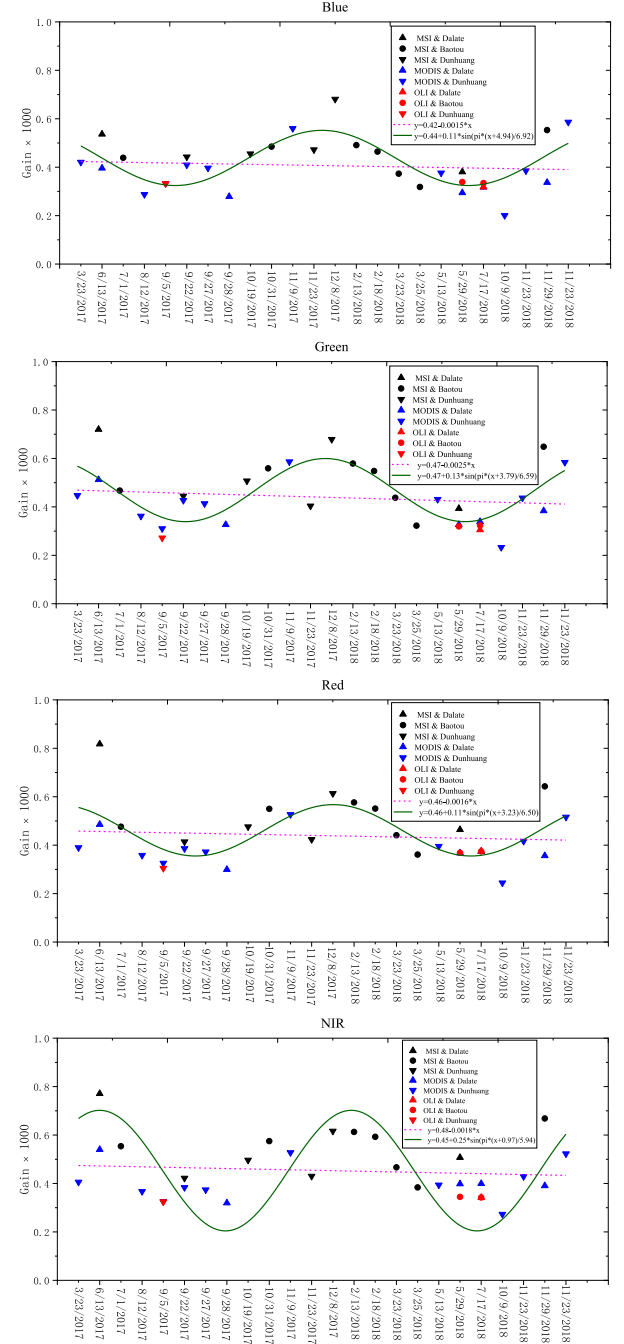
Fig. 14. Cross-calibration coefficients of GF-4/VNIR during 2017 and 2018.

MODTRAN 5 model (denoted as $\rho^*_{1,v}$) and is compared with two types of observed TOA reflectance. One is calculated according to the DN value extracted from the GF-4/VNIR images over the ground target and the calibration coefficients published by China Centre for Resources Satellite Data and Application (CRESDA) (denoted as $\rho^*_{1,p}$), the other one is calculated with DN value and the derived cross-calibration coefficients in this study (denoted as $\rho^*_{1,c}$). The validation results are shown in Fig. 15. Note that the $\rho^*_{1,c}$ is much closer to $\rho^*_{1,v}$ than $\rho^*_{1,p}$, and the maximum difference between $\rho^*_{1,c}$ and $\rho^*_{1,v}$ decreases from 28.5% to 15.4%. This

Fig. 15. Validation results with in situ synchronous measurements over Baotou site.

illustrates that the gain factors derived by cross-calibration are reasonable.

V. UNCERTAINTY ANALYSIS

In this study, the uncertainty contributions affecting the accuracy of cross-calibration of satellite sensors are related to three main domains: spectral, spatial, and angular. Although the view 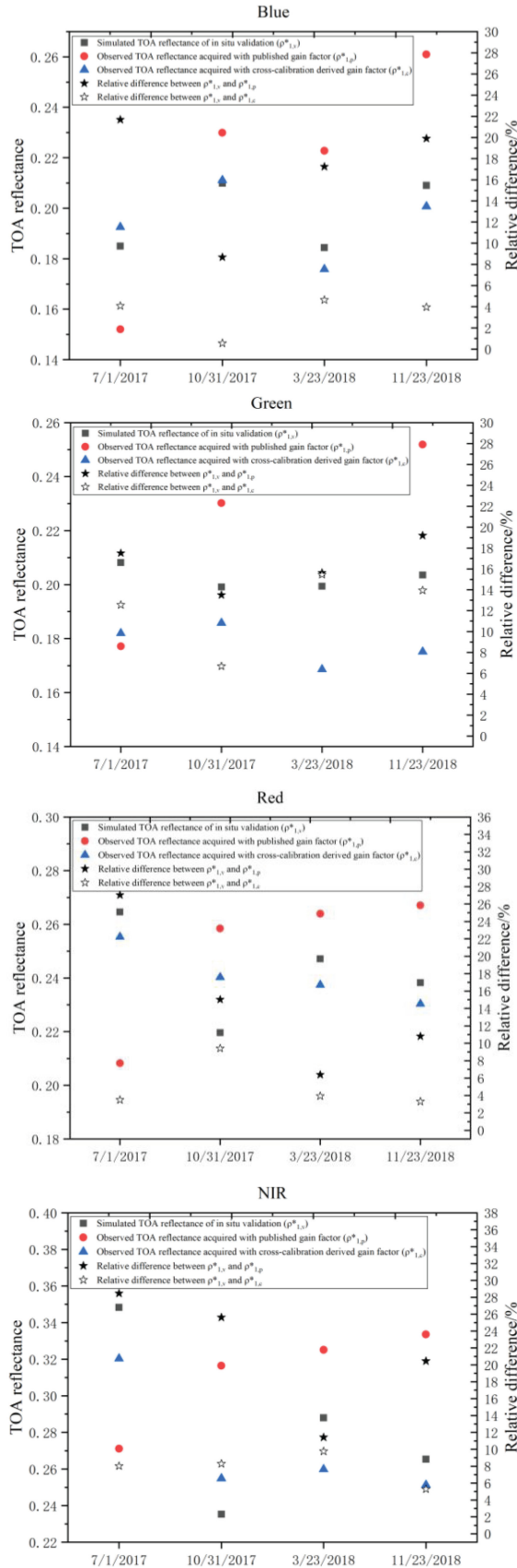geometries and spectral discrepancies between two sensors are reduced as much as possible, several factors, such as the uncertainty of the BRDF model, the uncertainties from WVC, AOD, aerosol type, and image registration, the uncertainty of MODTRAN model, are mentioned. Since some terms of uncertainty could not be quantified, a rough estimation is clarified as follows. The uncertainties analysis result of the cross-calibration against OLI, MSI, MODIS over Dunhuang, Dalate, and Baotou sites is shown in Tables II–IV.

1) The uncertainty caused by the referenced sensor calibration (denoted as σ_{cal})

The calibration uncertainty of Landsat8/OLI, Sentinel-2/MSI, and Terra/MODIS is approximately 3%, 3%, and 2%, respectively (see the third row in Tables II–IV) [22]–[24].

2) The uncertainty caused by the MODTRAN model (denoted as σ_m)

The uncertainty of the MODTRAN model is estimated to be approximately 2% [25], and according to the error transfer theory, this term of uncertainty is transferred independently to the cross-calibration results (see the fourth row in Tables II–IV).

3) The uncertainty caused by the BRDF effect (denoted as σ_{brf})

The uncertainty of the fitted Ross-Li BRDF model is approximately 5% over Dunhuang, Dalate, and Baotou sites, respectively, this term of uncertainty results in an uncertainty of 4.92% to the cross-calibration, and the uncertainty depends on wavelength and site characteristics (see the fifth row in Tables II–IV).

4) The uncertainty caused by WVC (denoted as σ_{wvc})

To investigate the effect of WVC uncertainty, the Monte-Carlo method as described in Supplement 1 to the Guide to the Expression of Uncertainty in Measurement (GUM) [26] is used. A Gaussian distribution with a mean of actual WVC value and a standard deviation of 12% of WVC is added to the original WVC when generating the simulated TOA reflectance in the GF-4/VNIR band. Running the Monte-Carlo simulation using $M = 1000$ trails would lead to a calibration uncertainty component, which is caused by the WVC uncertainty. The analysis results are shown in the sixth row in Tables II–IV. Note that the uncertainty of WVC contributes much lower to the total calibration uncertainty than that of BRDF, the maximum values are approximately 0.63%.

5) The uncertainty caused by AOD (denoted as σ_{aod})

Similar to the analysis method of WVC, a Gaussian distribution with a mean of actual AOD value and a standard deviation of 0.01 is added to the measured AOD @ 550 nm when generating the simulated TOA reflectance in the GF-4/VNIR band. The analysis results are shown in the seventh row in Tables II–IV. It is

TABLE II
UNCERTAINTY OF THE CROSS-CALIBRATION OF GF-4/VNIR WITH SENTINEL-2/MSI, LANDSAT8/OLI, AND TERRA/MODIS AT DUNHUANG SITE

Sources	Cross-calibration with MSI				Cross-calibration with OLI				Cross-calibration with MODIS			
	Blue	Green	Red	NIR	Blue	Green	Red	NIR	Blue	Green	Red	NIR
Calibration accuracy of referenced sensor	3.00%	3.00%	3.00%	3.00%	3.00%	3.00%	3.00%	3.00%	2.00%	2.00%	2.00%	2.00%
MODTRAN 5	2.00%	2.00%	2.00%	2.00%	2.00%	2.00%	2.00%	2.00%	2.00%	2.00%	2.00%	2.00%
BRDF	3.25%	3.83%	4.51%	4.78%	3.38%	4.14%	4.51%	4.83%	2.95%	4.05%	4.51%	4.84%
WVC	0.01%	0.02%	0.09%	0.42%	0.02%	0.08%	0.19%	0.06%	0.01%	0.03%	0.20%	0.25%
AOD@550nm	0.37%	0.30%	0.06%	0.12%	0.12%	0.02%	0.03%	0.09%	0.42%	0.29%	0.14%	0.11%
Aerosol type	0.37%	0.46%	0.19%	0.26%	1.09%	0.35%	0.32%	1.53%	0.49%	0.63%	0.99%	1.91%
Co-registration	0.04%	0.04%	0.04%	0.04%	0.03%	0.11%	0.26%	0.40%	0.18%	0.19%	0.24%	0.29%
Total uncertainty	4.80%	5.38%	5.90%	6.11%	4.96%	5.63%	5.90%	6.27%	3.90%	5.01%	5.54%	6.00%

TABLE III
UNCERTAINTY OF THE CROSS-CALIBRATION OF GF-4/VNIR WITH SENTINEL-2/MSI, LANDSAT8/OLI, AND TERRA/MODIS AT DALATE SITE

Sources	Cross-calibration with MSI				Cross-calibration with OLI				Cross-calibration with MODIS			
	Blue	Green	Red	NIR	Blue	Green	Red	NIR	Blue	Green	Red	NIR
Calibration accuracy of referenced sensor	3.00%	3.00%	3.00%	3.00%	3.00%	3.00%	3.00%	3.00%	2.00%	2.00%	2.00%	2.00%
MODTRAN 5	2.00%	2.00%	2.00%	2.00%	2.00%	2.00%	2.00%	2.00%	2.00%	2.00%	2.00%	2.00%
BRDF	3.12%	3.96%	4.67%	4.90%	3.22%	4.27%	4.62%	4.89%	2.60%	4.06%	4.61%	4.92%
WVC	0.02%	0.04%	0.14%	0.63%	0.02%	0.08%	0.19%	0.06%	0.01%	0.02%	0.17%	0.21%
AOD@550nm	0.31%	0.14%	0.09%	0.18%	0.17%	0.01%	0.10%	0.14%	0.68%	0.44%	0.13%	0.16%
Aerosol type	0.48%	0.64%	1.47%	2.24%	0.77%	0.76%	0.98%	1.32%	0.69%	0.69%	1.29%	2.31%
Co-registration	0.04%	0.07%	0.11%	0.14%	0.24%	0.54%	0.59%	0.18%	0.18%	0.35%	0.59%	0.17%
Total uncertainty	4.89%	5.30%	5.96%	6.43%	5.00%	5.54%	5.87%	6.19%	4.20%	5.01%	5.49%	6.07%

TABLE IV
UNCERTAINTY OF THE CROSS-CALIBRATION OF GF-4/VNIR WITH SENTINEL-2/MSI, LANDSAT8/OLI AT BAOTOU SITE

Sources	Cross-calibration with MSI				Cross-calibration with OLI			
	Blue	Green	Red	NIR	Blue	Green	Red	NIR
Calibration accuracy of referenced sensor	3.00%	3.00%	3.00%	3.00%	3.00%	3.00%	3.00%	3.00%
MODTRAN 5	2.00%	2.00%	2.00%	2.00%	2.00%	2.00%	2.00%	2.00%
BRDF	2.68%	3.47%	4.45%	4.78%	3.45%	4.38%	4.67%	4.90%
WVC	0.04%	0.07%	0.21%	0.81%	0.01%	0.03%	0.08%	0.02%
AOD@550nm	0.60%	0.48%	0.13%	0.04%	0.43%	0.20%	0.11%	0.14%
Aerosol type	0.93%	1.09%	1.46%	2.08%	1.60%	1.60%	2.01%	2.67%
Co-registration	0.11%	0.15%	0.16%	0.14%	0.07%	0.08%	0.09%	0.06%
Total uncertainty	4.65%	5.15%	5.92%	6.39%	5.26%	5.90%	6.24%	6.64%

worth noting that the uncertainty of AOD contributes much more to the total calibration uncertainty in the blue band than that in the other three bands, and the maximum values are approximately 0.68%.

6) The uncertainty caused by aerosol type (denoted as σ_{typ})

The three sites have a mixed aerosol type of the rural and desert models, whereas the rural aerosol type is selected in this study while simulating TOA reflectance, which would result in an error in the simulated TOA reflectance. In order to analyze the uncertainty caused by different aerosol types, a new group of

simulated TOA reflectance is generated when the desert aerosol model is used, and the relative differences are also computed, which is denoted as the uncertainty caused by aerosol type. It is noted that the maximum uncertainty caused by aerosol type is 2.67%.

7) Image coregistration error (denoted as σ_{reg})

Site nonuniformity in combination with uncertainty due to misregistration of image scenes, in principle, leads to a systematic uncertainty that needs to be accountable for the total uncertainty budget of this cross-calibration. In this study, a

sliding window method [27] is used to estimate that the image coregistration error would cause an uncertainty of approximately within 0.59% (see the eighth row in Tables II–IV).

According to the law of propagation of uncertainties, the total uncertainty σ could be calculated for each band, namely $\sigma = \sqrt{\sigma_{\text{cal}}^2 + \sigma_m^2 + \sigma_{\text{brf}}^2 + \sigma_{\text{wvc}}^2 + \sigma_{\text{aod}}^2 + \sigma_{\text{typ}}^2 + \sigma_{\text{reg}}^2}$ (see the ninth row in Tables II–IV). It is noted that the total uncertainty is approximately 3.9%–6.64%.

VI. Conclusion

In this study, a cross-calibration approach has been formulated and implemented to use image pairs from the tandem configuration period to radiometrically calibrate the GF-4/VNIR with respect to the Landsat8/OLI, Sentinel-2/MSI, and Terra/MODIS. In consideration of angular and spectral differences between two sensors, the angular difference is compensated with the aid of MODTRAN a radiative transfer model and Ross-Li BRDF model, and meanwhile, a simulation method is proposed to correct the spectral differences, so that a more accurate cross-calibration between the sensors can be performed. The results show that there is test site dependency and sensor dependency, and cross-calibration coefficients in the four bands roughly have similar variation trend as a sinusoidal function during 2017 and 2018, varying from 0.00023 to 0.00079. Furthermore, an uncertainty analysis related to the uncertainty of the BRDF model, the uncertainties from WVC and AOD, image registration, the uncertainty of MODTRAN model, are mentioned. The uncertainty results show that the calibration accuracy of referenced sensors, and the uncertainty of MODTRAN model, and BRDF uncertainty are the three main factors affecting the cross-calibration accuracy, the uncertainty caused by WVC, AOD, and the image co-registration error is low than 1%, respectively. The total uncertainty is approximately 3.9%–6.64%.

This work will benefit for the improvements to GF-4/VNIR in-orbit calibration and would go hand in hand with an improved understanding of surface reflectance characterization.

Acknowledgment

References

[1] P. M. Teillet, G. Fedosejevs, K. J. Thome, and J. L. Barker, "Impacts of spectral band difference effects on radiometric cross-calibration between satellite sensors in the solar-reflective spectral domain," *Remote Sens. Environ.*, vol. 110, no. 3, pp. 393–409, Oct. 2007.

[2] S. B. Duan, Z. L. Li, and P. Leng, "A framework for the retrieval of all-weather land surface temperature at a high spatial resolution from polar-orbiting thermal infrared and passive microwave data," *Remote Sens. Environ.*, vol. 195, pp. 107–117, Jun. 2017.

[3] S.B. Duan, Z. L. Li, B.H. Tang, H. Wu, and R.L. Tang, "Generation of a time-consistent land surface temperature product from MODIS data," *Remote Sens. Environ.*, vol. 140, pp. 339–349, Jan. 2014.

[4] M. Dinguirard and P. N. Slater, "Calibration of space-multispectral imaging sensors: A review," *Remote Sens. Environ.*, vol. 68, no. 3, pp. 194–205, Jan. 1999.

[5] P. M. Teillet, J. L. Barker, B. L. Markham, R. R. Irish, G. Fedosejevs, and J.C. Storey, "Radiometric cross-calibration of the Landsat-7 ETM+ and Landsat-5 TM sensors based on tandem data sets," *Remote Sens. Environ.*, vol. 78, no. 1, pp. 39–54, Oct. 2001.

[6] C. X. Gao et al., "An investigation of a novel cross-calibration method of FY-3C VIRR against NPPVIIRS in the Dunhuang test site," *Remote Sens.*, vol. 8, no. 2, pp. 1–13, Jan. 2016.

[7] F. Sakuma, M. Kikuchi, H. Inada, and S. Akagi, "Onboard calibration status of the ASTER instrument," in *Proc. SPIE*, 2012, pp. 85280W–1 –85280W–10.

[8] C. Cao, F. Weng, M. Goldberg, and X. Wu, "Intersatellite calibration of polar-orbiting radiometers using the SNO/SCO method," in *Proc. IGARSS*, 2005, pp. 109–112.

[9] K. J. Thome, J. M. Corkel, and J. Czapla-Myers, "In-situ transfer standard and coincident-view intercomparisons for sensor cross-calibration." *IEEE Trans. Geosci. Remote Sens.*, vol. 51, no. 3, pp. 1088–1097, Mar. 2013.

[10] C. Cao, S. Uprety, and S. Blonski, "Establishing radiometric consistency among VIIRS, MODIS, and AVHRR using SNO and SNOx methods," in *Proc. IGARSS*, 2012, pp. 6928–6931.

[11] P. M. Teillet et al., "A generalized approach to the vicarious calibration of multiple Earth observation sensors using hyperspectral data," *Remote Sens. Environ.*, vol. 77, no. 3, pp. 304–327, Sep. 2001.

[12] J. J. Liu, Z. Li, Y. L. Qiao, Y. J. Liu, and Y. X. Zhang, "A new method for cross-calibration of two satellite sensors," *Int. J. Remote Sens.*, vol. 25, no. 23, pp. 5267–5281, 2004.

[13] D. Wang and H. He, "Observation capability and application prospect of GF-4 satellite," in *Proc. 3rd Int. Symp. Space Opt. Instrum. Appl.*, 2017, vol. 192, pp. 393–401.

[14] Y.K. Liu et al., "Vicarious radiometric calibration/validation of Landsat-8 operational land imager using a ground reflected radiance-based approach with Baotou site in China," *J. Appl. Remote Sens.*, vol. 11, no. 4, 2017, Art. no. 044004.

[15] K. D. Knobelspiesse, B. Cairns, B. Schmid, M. O. Román, and C. B. Schaaf, "Surface BRDF estimation from an aircraft compared to MODIS and ground estimates at the Southern Great Plains site," *J Geophys. Res. Atmos.*, vol. 113, no. 20105, pp. 1–21, Oct. 2008.

[16] X. Li and A. Strahler, "Geometric-optical bidirectional reflectance modeling of the discrete crown vegetation canopy: Effect of crown shape and mutual shadowing," *IEEE Trans. Geosci. Remote Sens.*, vol. 30, no. 2, pp. 276–292, Mar. 1992.

[17] J. Ross, The Radiation Regime and Architecture of Plant Stands. Hingham, MA, USA: Dr W. Junk, 1981.

[18] D. Hadjimitsis, Z. Mitraka, I. Gazani, A. Retalis, N. Chrysoulakis, and S. Michaelides, "Estimation of spatio-temporal distribution of precipitable water using MODIS and AVHRR data: A case study for Cyprus," *Adv. Geosci.*, vol. 30, pp. 23–29, May 2011.

[19] Q. B. Pham, T. C. Yang, C. M. Kuo, and H. W. Tseng, "Combing random forest and least square support vector regression for improving extreme rainfall downscaling," *Water*, vol. 11, no. 3, Mar. 2019, Art. no. 451.

[20] J. M. Jackson et al., "Suomi-NPP VIIRS aerosol algorithms and data products," *J. Geophys. Res. Atmos.* vol. 118, no. 22, pp. 12673–12689, Oct. 2013.

[21] K. Arai, "Vicarious calibration based cross calibration of solar reflective channels of radiometers onboard remote sensing satellite and evaluation of cross calibration accuracy through band-to-band data comparisons," *Int. J. Adv. Comp. Sci. Appl.*, vol. 4, no. 3, pp. 67–74, 2013.

[22] B. Markham et al., "Landsat-8 operational land imager radiometric calibration and stability," *Remote Sens.*, vol. 6, no. 12, pp. 112275–12308, Dec. 2014.

[23] F. Gascon et al., "Copernicus sentinel-2 calibration and products validation status," *Remote Sens.*, vol. 9, pp. 584–665, Jun. 2017.

[24] B. Guenther et al., "Prelaunch algorithm and data format for the Level 1 calibration products for the EOS-AM1 moderate resolution imaging spectroradiometer (MODIS)," *IEEE Trans. Geosci. Remote Sens.*, vol. 36, no. 4, pp. 1142–1151, Jul. 1998.

[25] A. Berk, G. Anderson, P. Acharya, and E. Shettle, "MODTRAN5 5.2.1 user's manual," Spectral Sciences Inc., Air Force Research Laboratory, Burlington, MA, USA and Hanscom AFB, MA, USA. 2011.

[26] BIPM, IEC, IFCC, ILAC, ISO, IUPAC, IUPAP, OIML, "Supplement1 to the 'Guide to the expression of uncertainty in measurement'—Propagation of distributions using a Monte Carlo method," JCGM 101, Sep. 2008.

[27] Z. Wang et al., "Uncertainty analysis of cross-calibration for HJ-1 CCD camera," *Sci. China*, vol. 56, no. 3, pp. 713–723, Mar. 2013.
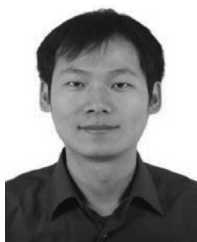
Caixia Gao received the B.S. degree in electronic and information engineering from the Xi'an University of Posts and Telecommunications, Xi'an, China, in 2006, the M.S. degree in computer science from the Academy of Opto-Electronics, Chinese Academy of Sciences, Beijing, China, in 2009, and the Ph.D. degree in cartography and geography information system from the University of Chinese Academy of Sciences, Beijing, China, in 2012.

She is currently an Associate Professor with the Aerospace Information Research Institute, Chinese Academy of Sciences. Her research interests include in-orbit calibration and validation of optical sensors, and the retrieval of surface temperature and emissivity.

Yaokai Liu received the Ph.D. degree in signal and information system from University of Chinese Academy of Sciences, Beijing, China, in 2018.

He is currently an Assistant Professor with Aerospace Information Research Institute, Chinese Academy of Sciences. His research interests include spectral and radiometric calibration of optical sensors, hyperspectral data processing and analysis, aerosol optical thickness and land surface reflectance from remote sensing data.

Shi Qiu received the B.S. degree from the Huazhong University of Science and Technology, Wuhan, China, in 2007, and the Ph.D. degree from the University of Strasbourg, Strasbourg, France, in 2013.

From 2014 to 2016, she was a Post-Doctor in cartography and geographical information system with the University of Maryland, Chinese Academy of Sciences, College Park, MD, USA. She has been selected as a member of the Hundred-Talent Program of Chinese Academy of Sciences. She is currently an Associate Professor with the Aerospace Information Research Institute, Chinese Academy of Sciences. Her research interests focus on in-orbit calibration of low-light sensors, and the quantitative applications of low-light remotely sensed data.

Chuanrong Li received the B.S. degree in aerocraft configuration mechanics from University of Science and Technology of China, Hefei, China, the master's degree in remote sensing from the University of Chinese Academy of Sciences, Beijing, China, in 1985, and the postgraduate degree from International Institute for Geoinformation Science and Earth Observation (ITC), Enschede, The Netherlands, in 1990.

He has been a Senior Visiting Scholar with CCRS from 1994 to 1995. From 1987 to 2003, he was a Research Scientist with the Remote Sensing Satellite Ground Station, Chinese Academy of Sciences (CAS), Beijing, China. Since 2003, he has been with the Academy of Opto-Electronics, CAS, as Vice President and Research Scientist. His research interests include remote sensing satellite ground systems and algorithms of remote sensing image processing.

Lingling Ma received the M.S. and Ph.D. degrees in geography and geographical information system from the Chinese Academy of Sciences, Beijing, China, in 2005 and 2008, respectively.

She is currently a Professor with the Aerospace Information Research Institute, Chinese Academy of Sciences. Her research interests include calibration and validation techniques of remote sensing data and products, and inflight performance assessment of optical sensors.

Qijin Han received the B.S. degree in mechanical and electronics engineering from Chang'an University, Xi'an, China, in 2007, and the M.S. degree in aircraft design from the China Academy of Space Technology, Beijing, China, in 2010.

He is currently an Associate Professor with the China Center for Resources Satellite Data and Application, Beijing, China. His research interests include radiometric calibration and validation of remote sensors, data processing, and quantitative applications of remotely sensed images.

Jingru Liu received the B.S. degree in remote sensing science and technology from Shandong University of Science and Technology, Qingdao, China, in 2017. He is currently working toward the postgraduate degree in electronics and communication engineering at Aerospace Information Research Institute, Chinese Academy of Sciences.

His research interest focuses on the vicarious radiometric calibration of optical sensors.

Enyu Zhao received the Ph.D. degree from the College of Resources and Environment, University of Chinese Academy of Sciences, Beijing, China, in 2017, and the joint Ph.D. degree in cartography and geographic information system from the University of Chinese Academy of Sciences, Beijing, China, and the Engineering Science, Computer Science and Imaging Laboratory, University of Strasbourg, Strasbourg, France.

He is currently a Lecturer with the College of Information Science and Technology, Dalian Maritime University, Dalian, China. His research interests include remote sensing and hyperspectral image processing.

Yongguang Zhao received the B.S. degree in geographic information system from Central South University, Changsha, China, in 2009, and the Ph.D. degree in signal and information processing from the Academy of Opto-Electronics, Chinese Academy of Sciences, Beijing, China, in 2015.

He is currently an Associate Professor with the Aerospace Information Research Institute, Chinese Academy of Sciences. His research interests include radiometric calibration and quantitative remote sensing application.

Yonggang Qian received the B.S. degree in applied mathematics from Yantai University, Yantai, China, in 2003, the M.S. degree in geographical information system from Taiyuan University of Technology, Taiyuan, China, in 2006, and the Ph.D. degree in cartography and geographical information system from Beijing Normal University, Beijing, China, in 2009.

He was a Post-Doctor in cartography and geographical information system with the Institute of Geographic Sciences and Natural Resources Research, Chinese Academy of Sciences, Beijing, China, from 2009 to 2011. He is currently a Professor with the Aerospace Information Research Institute, Chinese Academy of Sciences. His research interests include the retrieval and validation of surface temperature and emissivity from remotely sensed data.

Ning Wang received the B.S. and M.S. degrees in geophysical science and cartography and geographic information system from the Beijing Normal University, Beijing, China, in 2004 and 2007, respectively, and the Ph.D. degree in cartography and geographical information system from the Institute of Geographic Sciences and Natural Resources Research, Chinese Academy of Sciences, Beijing, China, in 2011.

He is currently a Professor with the Aerospace Information Research Institute, Chinese Academy of Sciences. His research interests include in-orbit calibration of optical sensors, and hyperspectral remote sensing.